

# Fabrication of Porous Fe/TiB<sub>2</sub> Composites by Reactive Precursor Method

Osayoshi Kato

Graduate School of Engineering, Nagoya University

1 Fro-cho, Chikusa-ku, Nagoya 4648603, Japan

Makoto Kobashi (Corresponding author) & Naoyuki Kanetake

Department of Materials Science and Engineering, Nagoya University

1 Fro-cho, Chikusa-ku, Nagoya 4648603, Japan

Tel: 81-52-789-3356 E-mail: kobashi@numse.nagoya-u.ac.jp

Received: January 13, 2012 Accepted: February 1, 2012 Published: April 1, 2012

doi:10.5539/jmsr.v1n2p110

URL: <http://dx.doi.org/10.5539/jmsr.v1n2p110>

*This study was supported by JFE 21st Century Foundation.*

## Abstract

Porous Fe/TiB<sub>2</sub> composites were fabricated by a reactive precursor method. Fundamentally, iron, titanium and boron powders were blended to synthesize 20 to 70 vol% TiB<sub>2</sub> particles in Fe/TiB<sub>2</sub> composites after the combustion reaction. Additionally, various foaming agent powders (CaCO<sub>3</sub>, MgCO<sub>3</sub>, SrCO<sub>3</sub>, TiH<sub>2</sub>, ZrH<sub>2</sub> and C) were added to the blended powder. The blended powder compact was heated to induce the combustion reaction. The specimen prepared with carbon had large pores and high porosity (the maximum porosity was 60% and the pore size was about 800 μm). The reasons why the porosity increases are twofold; (i) the melting point of iron is decreased by carburizing and (ii) carbon is oxidized during the combustion process and the formation of gaseous CO results in generating the pores.

**Keywords:** Metallic foam, Porous metal, Powder metallurgy, Combustion synthesis, Composite, Steel, Titanium diboride

## 1. Introduction

Porous metals have unique properties such as high-specific stiffness, damping capacity, heat insulating effect and so forth. By these characteristics, they are expected to be applied to impact absorbers, sound absorption panels and compact heat exchangers (Banhart, 2001). Porous aluminum alloys have been studied by many researchers (Chino, *et al.*, 2002; Duarte, *et al.*, 2000; Matijasevic, *et al.*, 2006), and nowadays iron based porous metals are also researched since they possess several attractive properties such as high strength, high stiffness, high melting temperature and compatibility with steel components (Park, *et al.*, 2000; Park, *et al.*, 2001 a; Park, *et al.*, 2001b; Park, *et al.*, 2002; Stephani, *et al.*, 2005). However, there are some difficulties to manufacture iron based porous materials. For example, high temperature near the melting point of iron is required for the fabrication, and the drainage occurs easily because the specific gravity of iron is larger than that of aluminum.

The authors have developed an innovative manufacture process, “reactive precursor method”, in which the precursors consisting of at least two elemental powders are used (Inoguchi, *et al.*, 2009; Kanetake, *et al.*, 2006; Kobashi, *et al.*, 2002; Kobashi, *et al.*, 2006; Kobashi, *et al.*, 2010). The elemental powders should react with each other and release high heat of formation to let the combustion reaction happen. Once the combustion reaction occurs, inorganic compounds (ceramics or intermetallics) are synthesized and the temperature of the reaction products increases rapidly due to the heat of formation. It is known that the specimens after the combustion reaction are usually porous. The residual atmospheric gas originally existed in the precursor and the released gases originally adsorbed at or absorbed in the elemental powders are main sources of the pores. Since the combustion reaction generates large amount of heat, the specimen’s temperature is much higher than the

atmospheric temperature during the reaction. Therefore the cooling rate is very fast and solidification occurs rapidly. This is also an advantageous feature to avoid the severe drainage (Park, *et al.*, 2000).

In this research, we chose three elemental powders (iron, titanium and boron) as starting powders. By heating the blended [Fe+Ti+B] powder, a combustion reaction shown below occurs.



Where  $\alpha$  is mole fraction of  $\text{TiB}_2$  in Fe/ $\text{TiB}_2$  composite.

By changing the value of  $\alpha$  in eq. (1), the volume fraction of  $\text{TiB}_2$  in the composite can be controlled. It is reported that  $\text{TiB}_2$  is thermodynamically stable in iron and suitable as the strengthening ceramics in iron (Tanaka, *et al.*, 1998 a). Aside from releasing the large amount of heat reaction,  $\text{TiB}_2$  particles play another important role to increase the viscosity of molten iron, which can stabilize the foam structure. Additionally, the interface bonding between iron and  $\text{TiB}_2$  is reported to be strong and the dispersion of  $\text{TiB}_2$  particles improves the stiffness of iron (Tanaka, *et al.*, 1998b).

The objective of this research is to develop a processing technique to manufacture porous Fe/ $\text{TiB}_2$  composites by the reactive precursor method. In this research, various kinds of foaming agents were added in order to control the pore morphology and porosity. We investigated the effect of the volume fraction of  $\text{TiB}_2$  in solid iron on the foaming behavior and also the effect of various foaming agent on porosity.

## 2. Experimental Procedure

Iron powder (3-5 $\mu\text{m}$ , 99.99%), titanium powder (<45 $\mu\text{m}$ , 99.9%) and boron powder (<45 $\mu\text{m}$ , 99%) were blended to synthesize 20 to 70 vol%  $\text{TiB}_2$  particles in Fe/ $\text{TiB}_2$  composites after the reaction (1). A foaming agent powder was added to the blended powder. Six kinds of foaming agents were prepared, and their effects on the foaming behavior were compared. The list of the foaming agents used in this experiment is shown in table 1. The additive amount of the foaming agents was fundamentally 1.0 mass%. Only the additive amount of carbon was varied from 1.0 to 5.0 mass%. The blended powder was compressed into a cylindrical shape ( $\phi 10 \times h 10$  mm) by a uniaxial cold-pressing (applied pressure: 200MPa). The relative density of the precursors was about 0.67. The precursor was heated in an induction furnace under an argon atmosphere to induce the combustion reaction shown in eq. (1) (heating rate 3.5°C/sec.). The specimen was cooled in the furnace immediately after the bright light emission of the combustion reaction was confirmed. The porosity of the specimen was measured by an Archimedes method. The cross section of the specimen was observed by a scanning electron microscope (SEM). The temperature profile during the combustion reaction was measured by inserting a thermocouple in the specimen. The carbon concentration in the iron powder was measured by a combustion-infrared absorptiometric method (LECO CS444). The quantitative analysis of the gas phase in the pore was carried out by mass spectrometry (ANELVA AGS-7000). Oxygen concentration in iron and titanium powder was measured by an inert gas fusion infrared absorption method (LECO TC 600).

## 3. Results and Discussion

### 3.1 Reaction between Fe, Ti and B Powder

Figure 1 shows the adiabatic temperatures of combustion ( $T_{ad}$ ) with various volume fractions of  $\text{TiB}_2$ . This thermodynamic parameter is the temperature to which the product is raised under adiabatic conditions as a consequence of the evolution of heat from the reaction (Munir, *et al.*, 1989). In this experiment, the adiabatic temperature was calculated by the following equation.

$$\Delta H_f + \int_{T_0}^{T_m} C_{p,Fe} dT + \Delta H_{melt,Fe} + \int_{T_m}^{T_{ad}} C_{p,Fe} dT + \int_{T_0}^{T_{ad}} C_{p,TiB_2} dT = 0 \quad (2)$$

Where  $\Delta H_f$  is the heat formation (J),  $T_0$  is the initial temperature (°C),  $T_m$  is the melting point of iron (°C),  $C_p$  is the constant pressure specific heat (J/(mol·°C)) and  $\Delta H_{melt,Fe}$  is the latent heat of iron at its melting point (J).

In order to fabricate closed-cell-type porous metals by the combustion process, the adiabatic temperature must exceed the melting point of the metal. This is because the pore formation and growth can occur only when sufficient amount of liquid phase is presented. According to the calculation shown in eq. (2), the adiabatic temperature exceeded the melting point of iron, when  $\text{TiB}_2$  volume fraction was over 20 vol%. However, when  $\text{TiB}_2$  volume fraction reached to 60 vol%, the adiabatic temperature exceeded the boiling point of iron. This extremely high adiabatic temperature often ended up with the explosion of the specimen during the combustion reaction. According to this calculation, we decided to carry out this experiment with  $\text{TiB}_2$  volume fractions in between 20 and 70 vol%.

Figure 2 shows the cross sections of the specimens with 20~70 vol% TiB<sub>2</sub>. When TiB<sub>2</sub> volume fraction was 20 vol%, the light emission of the combustion reaction was very weak and the closed pores were not observed. For the specimens with 30~60 vol% TiB<sub>2</sub>, the combustion reaction was clearly observed and closed pores were formed (pore sizes were about 1mm). The specimen with 70 vol% TiB<sub>2</sub> exploded. The explosion occurred because the maximum combustion temperature exceeded the boiling point of iron.

Figure 3 shows the microstructure of the solid section of the specimen (cell wall) with 50 vol% TiB<sub>2</sub>. TiB<sub>2</sub> particles (2-3µm) were uniformly dispersed in the iron matrix. This homogeneous dispersion of fine particles may be beneficial to improving the stability of pores due to an increased viscosity. Figure 4 shows the temperature profile during the combustion reaction. Ignition temperature was confirmed as 960°C. The ignition temperature was nearly constant (about 950°C) regardless of the volume fraction of TiB<sub>2</sub>. This implies that the porous Fe/TiB<sub>2</sub> composite can be manufactured at temperatures much lower than the melting temperature of iron. Although the maximum combustion temperature could not be measured precisely, it is apparent that the combustion reaction occurred in a short range of time. The temperature of the specimen exceeded the melting point of iron only for about 2 seconds, which is effective to prevent the severe drainage during the foaming process.

Based on the above results, we mainly researched the effect of foaming agents for the specimens with 30~60 vol%TiB<sub>2</sub> in the following section.

### 3.2 Effect of Various Foaming Agents

Figure 5 and Fig.6 show the cross sections and porosities of the specimens with various foaming agent additions (TiB<sub>2</sub> volume fraction: 50 vol%). The foaming agents other than carbon (CaCO<sub>3</sub>, MgCO<sub>3</sub>, SrCO<sub>3</sub>, TiH<sub>2</sub> and ZrH<sub>2</sub>) were expected to increase porosity due to the CO<sub>2</sub> or H<sub>2</sub> gas emission by the decomposition at high temperatures. But the results showed that porosities did not increase at all by adding these foaming agents. The pore size was not increased as well. This is probably because the decomposition temperatures of these foaming agents were not coincident with the temperature range of the combustion reaction (Table 2). Furthermore, the melting time was too short to allow a sufficient emission of gaseous phase from the foaming agents.

Apart from these foaming agents, carbon was expected to decrease the melting point of iron by carburizing. Furthermore, carbon was also expected to react with oxygen dissolved in the elemental powders during the combustion process and generate gaseous carbon oxide. As shown in Figures 5 and 6, it is apparent that the carbon added specimen exhibited larger pores and the higher porosity (48%). For investigating the carbon's role of increasing the porosity, the carbon concentration in iron after the reaction and the gas phase composition in the pores were measured. As a result, the carbon concentration in iron turned out to be 1.6 mass%. According to the Fe-C phase diagram, the liquidus temperature of Fe-C of this composition is about 1250°C. From this result, it is apparent that the melting temperature of the specimen was decreased by adding the carbon powder. Moreover, CO gas was detected in the gas extracted from the pores. Therefore, it is clear that carbon becomes CO gas and forms the pores. Since the chamber was filled with argon and there was little oxygen in the atmosphere, carbon was considered to be reacted with oxygen in the elemental powders. Then, oxygen concentrations in iron and titanium powders were measured. As a result of the analysis, iron and titanium powder contained 0.42 and 0.43 mass% oxygen, respectively. Assuming that all oxygen turns into CO gas, the volume of the emitted CO gas is about 50 times larger than the volume of the precursor. This implies that the amount of oxygen in the elemental powders was sufficient to form pores as shown in Figure 5.

### 3.3 Effect of Carbon Additive Amount

As indicated in 3.2, the carbon addition was effective to increase the porosity. Therefore, in this section, the effect of the carbon additive amount is discussed. Figure 7 shows cross sections of the specimens with 0~5.0 mass%C additions (TiB<sub>2</sub> volume fractions: 30~60 vol%). When carbon additive amounts were 1.0 and 2.0mass%, both the number of pores and the pore size were increased in comparison with the non-added specimen. The porosity of the specimen prepared with 50 vol% TiB<sub>2</sub> and 3.0 mass%C showed the highest porosity (60%). However, the closed pores were no longer formed by adding 3.0 and 4.0 mass%C when TiB<sub>2</sub> volume fractions were 30, 40% and 50%.

Figure 8 shows the porosities of the specimens with 1.0~3.0 mass%C additions. Porosities of the specimens with 1.0, 2.0 and 3.0 mass%C additions were 48%, 51% and 60%, respectively. Fig.9 shows the macroscopic and microscopic cross-sections of the specimen with the 3.0 mass%C addition. The pore size was about 800µm and the closed cell-structure was apparent (Fig.9 (a)). TiB<sub>2</sub> particles (2-3µm) were uniformly dispersed in the iron matrix (Fig.9 (b)). Fig.10 shows the microstructure of the specimen with 5.0 mass%C addition. The cell structure of the specimen changed to an open-cell type with the pore size under 100µm. Fig.11 shows calculated adiabatic

temperatures of the combustion synthesized specimen with various carbon additive amounts. According to Fig.11, it is apparent that the theoretical adiabatic temperature is not significantly affected by the carbon additive amount. This is because the specific heat of carbon is smaller than those of iron and titanium. Fig.12 shows temperature profiles of the specimens with 0, 3.0 and 5.0 mass% C additions. With respect to the practical temperature profile, the maximum combustion temperatures exceeded the melting point of iron when carbon additive amounts were 0 and 3.0 mass%, but the exothermic peak of the specimen with 5.0 mass% C addition dropped suddenly to the temperature below the melting point of iron, although the calculated adiabatic temperature was not significantly influenced by the carbon addition. In this case, the carbon powders ( $d=5\mu\text{m}$ ) spreading in between titanium and boron powders ( $d<45\mu\text{m}$ ) might hinder the direct contact of titanium and boron and, therefore, prevent the reaction.

#### 4. Conclusions

The processing technique for manufacturing porous Fe/TiB<sub>2</sub> composites by a reactive precursor method was investigated. The following results were obtained through the experiments.

- 1). For making porous Fe/TiB<sub>2</sub> composites by a reactive precursor method, carbon powder turned out to be a suitable foaming agent. The decreased melting point of Fe-C alloy and the generation of carbon monoxide gas are the main reasons for the increased porosity by adding carbon. Other powders (CaCO<sub>3</sub>, MgCO<sub>3</sub>, SrCO<sub>3</sub>, TiH<sub>2</sub> and ZrH<sub>2</sub>) were not effective to increase the porosity.
- 2). When TiB<sub>2</sub> volume fraction was 50% and carbon additive amount was 3.0 mass%, the porosity was 60% and the pore size was about 800 $\mu\text{m}$ . The microstructure of the solid section of the porous specimen showed TiB<sub>2</sub> particles (2-3 $\mu\text{m}$ ) uniformly dispersed in iron matrix.
- 3). By increasing the carbon additive amount up to 4.0~5.0 mass%, the carbon powders spreading in between titanium and boron powders might prevent the reaction and, therefore, the closed-cell structure could not be obtained.

#### References

- Banhart, J. (2001). Manufacture, characterization and application of cellular metals and metal foams. *Progress in Materials Science*, 46(6), 559-632. [http://dx.doi.org/10.1016/S0079-6425\(00\)00002-5](http://dx.doi.org/10.1016/S0079-6425(00)00002-5)
- Chino, Y., Nakanishi, H., Kobata, M., Iwasaki, H., & Mabuchi, M. (2002). Processing of a porous 7075 Al alloy by bubble expansion in a semi-solid state. *Scripta Materialia*, 47(11), 769-773. [http://dx.doi.org/10.1016/S1359-6462\(02\)00299-3](http://dx.doi.org/10.1016/S1359-6462(02)00299-3)
- Duarte, I., & Banhart, J. (2000). A study of aluminium foam formation-kinetics and microstructure. *Acta Materialia*, 48(9), 2349-2362. [http://dx.doi.org/10.1016/S1359-6454\(00\)00020-3](http://dx.doi.org/10.1016/S1359-6454(00)00020-3)
- Inoguchi, N., Kobashi, M., & Kanetake, N. (2009). Synthesis of Porous Al<sub>3</sub>Ti/Al Composite and Effect of Processing Condition on Cell Morphology. *Materials Transactions*, 50(11), 2609-2614. <http://dx.doi.org/10.2320/matertrans.L-M2009823>
- Kanetake, N., & Kobashi, M. (2006). Innovative processing of porous and cellular materials by chemical reaction. *Scripta Materialia*, 54(4), 521-525. <http://dx.doi.org/10.1016/j.scriptamat.2005.10.063>
- Kobashi, M., & Kanetake, N. (2002). Processing of intermetallics foam by combustion reaction. *Advanced Engineering Materials*, 4(10), 745-747. [http://dx.doi.org/10.1002/1527-2648\(20021014\)4:10<745::AID-ADEM745>3.0.CO;2-U](http://dx.doi.org/10.1002/1527-2648(20021014)4:10<745::AID-ADEM745>3.0.CO;2-U)
- Kobashi, M., Inoguchi, N., & Kanetake, N. (2010). Powder size effect on cell morphology of combustion synthesized porous Al<sub>3</sub>Ti/Al composite. *Intermetallics*, 18(5), 1102-1105. <http://dx.doi.org/10.1016/j.intermet.2009.12.033>
- Kobashi, M., Wang, R., Inagaki, Y., & Kanetake, N. (2006). Effects of processing Parameters on pore morphology of combustion synthesized Al-Ni foams. *Materials Transactions*, 47(9), 2172-2177. <http://dx.doi.org/10.2320/matertrans.47.2172>
- Matijasevic, B., & Banhart, J. (2006). Improvement of aluminium foam technology by tailoring of blowing agent. *Scripta Materialia*, 54(4), 503-508. <http://dx.doi.org/10.1016/j.scriptamat.2005.10.045>
- Munir, Z. A., & Anselmi-Tamburini, U. (1989). Self-propagating exothermic reactions: The synthesis of high-temperature materials by combustion. *Materials Science Reports*, 3(6), 277-365. [http://dx.doi.org/10.1016/S0920-2307\(89\)80002-7](http://dx.doi.org/10.1016/S0920-2307(89)80002-7)

- Park, C., & Nutt, S. R. (2000). PM synthesis and properties of steel foam. *Materials Science and Engineering*, A288(1), 111-118. [http://dx.doi.org/10.1016/S0921-5093\(00\)00761-9](http://dx.doi.org/10.1016/S0921-5093(00)00761-9).
- Park, C., & Nutt, S.R. (2001a). Anisotropy and strain localization in steel foam. *Materials Science and Engineering*, A299(1-2), 68-74. [http://dx.doi.org/10.1016/S0921-5093\(00\)01418-0](http://dx.doi.org/10.1016/S0921-5093(00)01418-0)
- Park, C., & Nutt, S. R. (2002). Strain rate sensitivity and defects in steel foam. *Materials Science and Engineering*, A323(1-2), 358-366. [http://dx.doi.org/10.1016/S0921-5093\(01\)01372-7](http://dx.doi.org/10.1016/S0921-5093(01)01372-7)
- Park, C., & Nutt, S. R. (2001b). Effects of process parameters on steel foam synthesis. *Materials Science and Engineering*, A297(1-2), 62-68. [http://dx.doi.org/10.1016/S0921-5093\(00\)01265-X](http://dx.doi.org/10.1016/S0921-5093(00)01265-X)
- Stephani, G., Andersen, O., Göhler, H., Kostmann, C., Kümmel, K., Quadbeck, P., Reinfried, M., Studnizky, T., & Waag, U. (2005). Iron Based Cellular Structures - Status and Prospects. *Advanced Engineering Materials*, 8(9), 847-852. <http://dx.doi.org/10.1002/adem.200600078>
- Tanaka, K., Oshima, T., & Saito, T. (1998a). Development of High Modulus Steel Based on Thermodynamic Phase Equilibrium between  $TiB_2$  and Ferrite. *The Iron and Steel Institute of Japan*, 84(8), 586-591.
- Tanaka, K., Oshima, T., & Saito, T. (1998b). Mechanical Properties and Hot-workability of  $TiB_2$ -reinforced High Modulus Steel. *The Iron and Steel Institute of Japan*, 84(10), 747-754.

Table 1. Size and purity of foaming agents

Powder	$CaCO_3$	$MgCO_3$	$SrCO_3$	$TiH_2$	$ZrH_2$	C
Size	1 $\mu m$	1 $\mu m$	1 $\mu m$	< 45 $\mu m$	5 $\mu m$	5 $\mu m$
Purity	99.99%	99.9%	99.9%	99%	98%	99.7%

Table 2. Decomposition temperatures of the foaming agents used in this research

Foaming agent	Decomposition temperature ( $^{\circ}C$ )
$TiH_2$	470~560
$MgCO_3$	525~600
$ZrH_2$	600~717
$CaCO_3$	600~800
$SrCO_3$	1250~1330

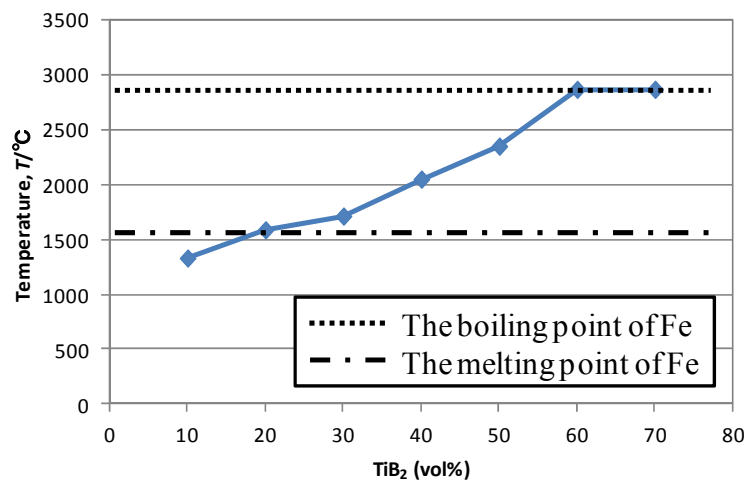


Figure 1. Adiabatic temperature of the combustion synthesized specimens as a function of TiB<sub>2</sub>

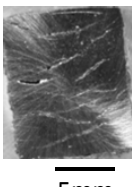

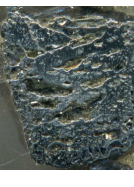
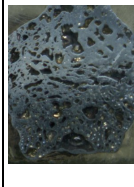
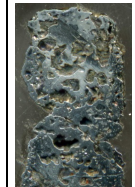

TiB <sub>2</sub>	20vol%	30vol%	40vol%	50vol%	60vol%	70vol%
Cross section of the specimen						

Figure 2. Cross sections of the combustion synthesized Fe/TiB<sub>2</sub> specimens with 20~70 vol% TiB<sub>2</sub>

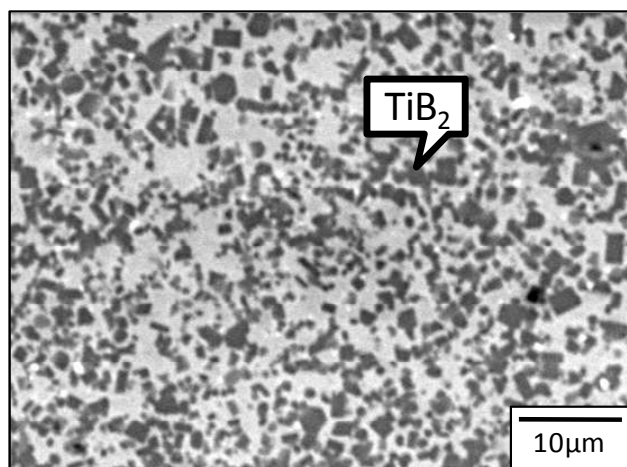


Figure 3. SEM micrograph of the combustion synthesized Fe/TiB<sub>2</sub> specimen of 50 vol% TiB<sub>2</sub>

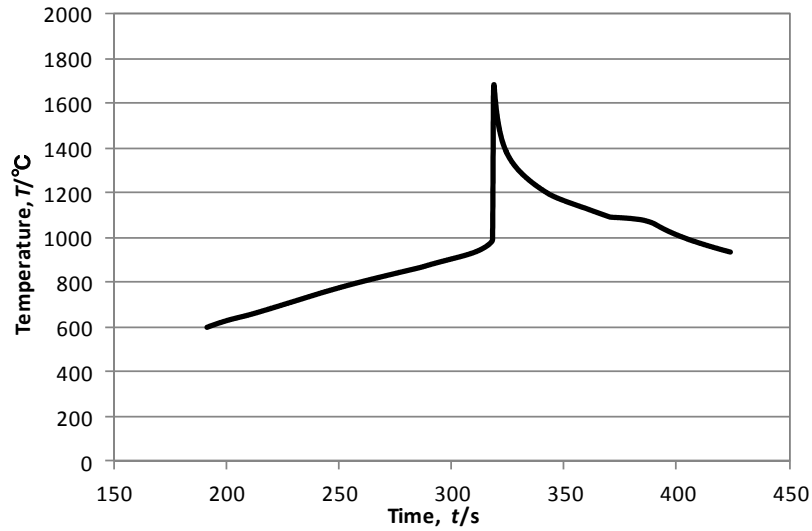


Figure 4. Temperature profile of the Fe-50 vol%TiB<sub>2</sub> specimen

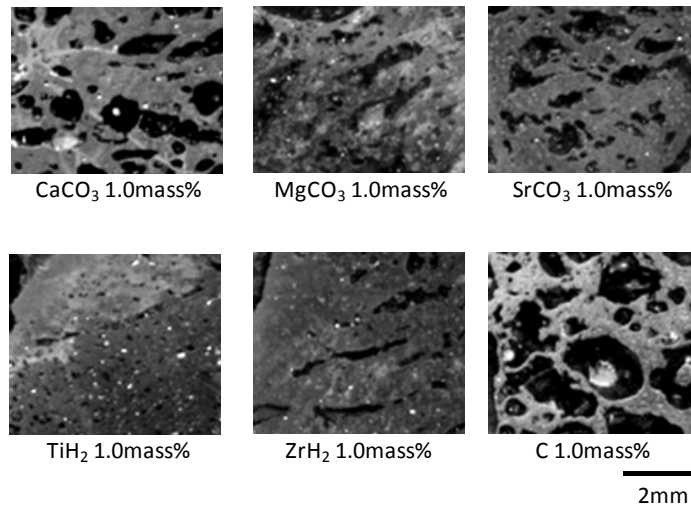


Figure 5. Cross sections of the specimens with 1.0 mass% addition of the foaming agents (TiB<sub>2</sub> volume fraction: 50 vol%)

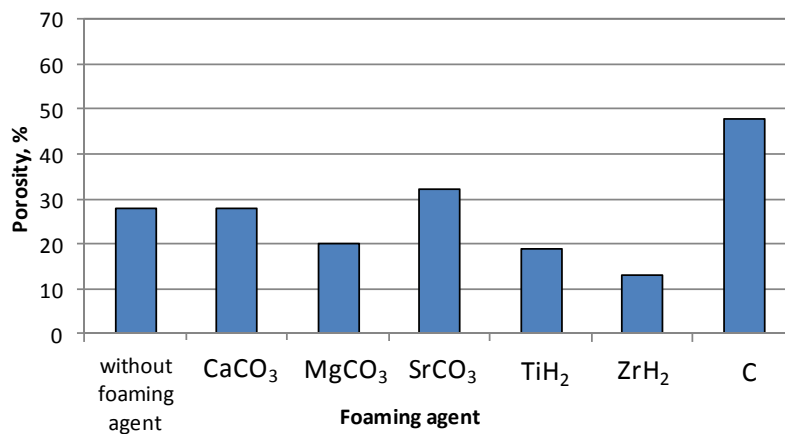


Figure 6. Porosities of the specimens with various foaming agent additions (TiB<sub>2</sub> volume fraction: 50 vol%)

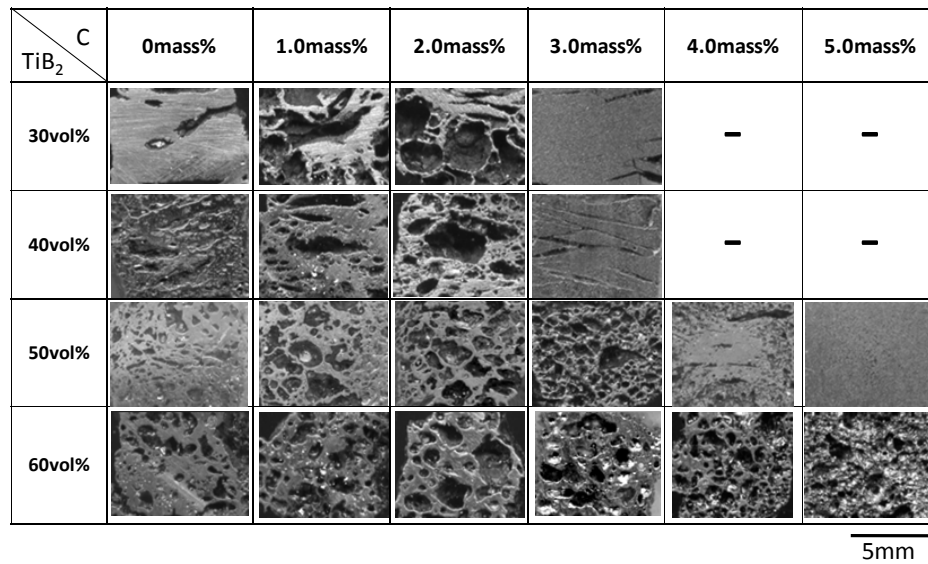


Figure 7. Cross sections of the specimens with 0~5.0 mass%C additions ( $\text{TiB}_2$  volume fraction: 30~60 vol%)

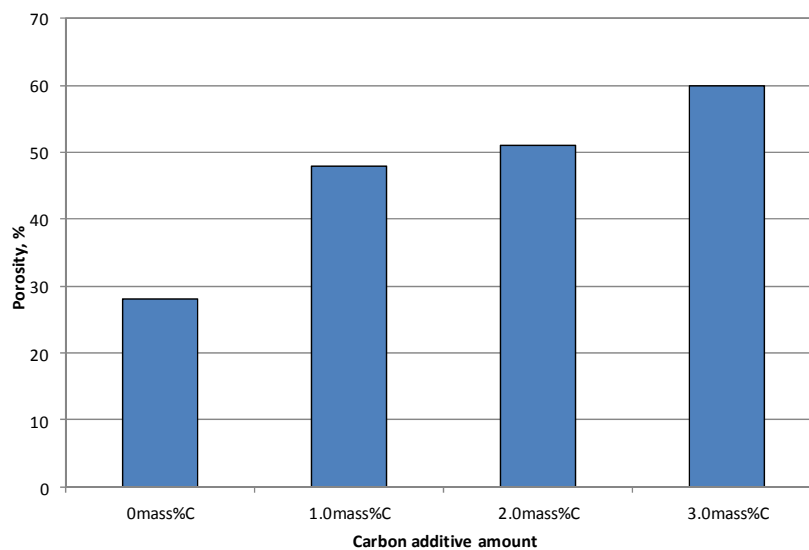


Figure 8. Porosities of the specimens with 0~3.0 mass%C additions ( $\text{TiB}_2$  volume fraction: 50 vol%)

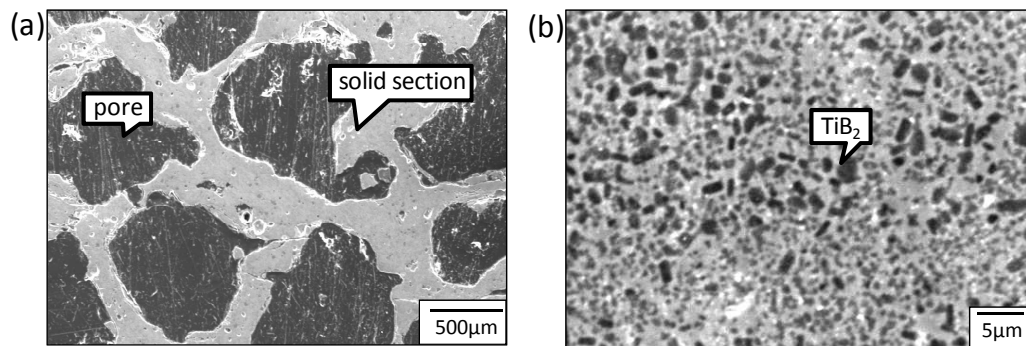


Figure 9. SEM micrographs of the specimen with a 3.0 mass%C addition ( $\text{TiB}_2$  volume fraction: 50 vol%). (a) Macroscopic cross-section and (b) microstructure



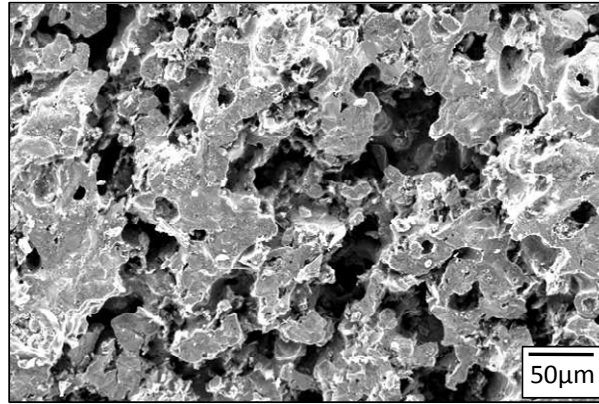


Figure 10. SEM micrograph of the specimen with 5.0 mass% C addition ( $\text{TiB}_2$  volume fraction: 50 vol%)

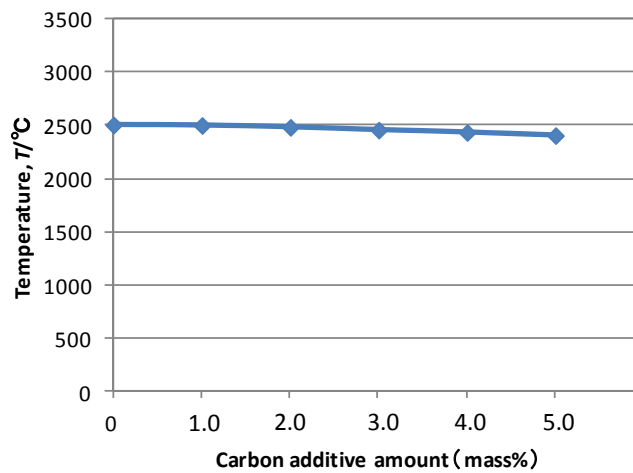


Figure 11. Adiabatic temperatures of the combustion synthesized specimens with various carbon additive amounts ( $\text{TiB}_2$  volume fraction: 50 vol%)

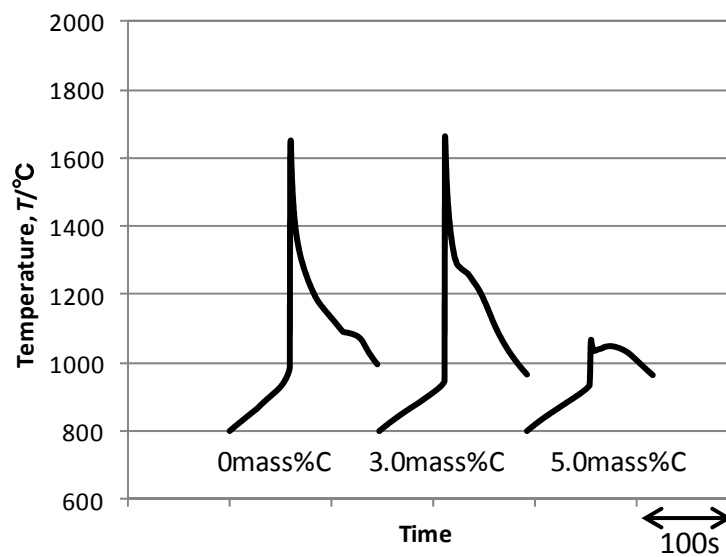


Figure 12. Temperature profiles of the specimens with various carbon additive amounts ( $\text{TiB}_2$  volume fraction: 50 vol%)